Int. J. Heat Mass Transfer. Vol. 30, No. 12, pp. 2539–2548, 1987
Printed in Great Britain

0017 9310/87 $3.00 + 0.00
Pergamon Journals Ltd.

Natural convection in V-shaped and L-shaped corners

R. RUIZ and E. M. SPARROW
Department of Mechanical Engineering, University of Minnesota, Minneapolis, MN 55455, U.S.A.

(*Received* 17 *March* 1987 *and in final form* 26 *May* 1987)

Abstract—Experiments were performed to investigate convection in two types of corners. One, the V corner, is formed by two 45° inclined, upward-facing, heated plates which intersect at 90°. The other, the L corner, is formed by an upward-facing, heated horizontal plate which intersects with a heated vertical plate. In both cases, the two plates had the same uniform temperature which was varied parametrically. The variations of the surface-to-ambient temperature difference and of the plate length yielded a Rayleigh number range from 2×10^6 to 1.5×10^9. Apparatus modifications were also made to investigate the possible role of end effects. The heat transfer experiments were supplemented by flow visualization. The Nusselt numbers for all cases were amenable to power-law correlations with the Rayleigh number. The values of the Nusselt number at the walls of the V corner and at the horizontal wall of the L corner were greater than those for the counterpart single plates.

INTRODUCTION

THIS PAPER describes an experimental study of natural convection in two types of corners, each formed by the intersection of a pair of plane surfaces. The two corners are illustrated schematically in elevation view in Figs. 1(a) and (b). In both cases, the line of intersection of the participating plane surfaces is horizontal. The corner in Fig. 1(a) will be termed a V corner. It is formed by two upward-facing heated plates which intersect at 90°, with each plate inclined at 45° to the horizontal. Both plates were maintained at the same uniform temperature T_w which exceeded the ambient temperature T_∞, and both plates were of length L. The other corner is an L corner, Fig. 1(b), which is formed by an upward-facing heated horizontal plate which intersects with a heated vertical plate. Again, the two plates had a common uniform temperature T_w and both were of length L.

The experiments were performed in a thermally guarded water bath, with the temperature level set so that the nominal value of the Prandtl number was 5. The Rayleigh number was varied both by varying the plate dimension L and the wall-to-ambient temperature difference $(T_w - T_\infty)$. For the V corner, this resulted in a Rayleigh number range which extended from about 2×10^6 to 1.5×10^9. The range for the L corner was slightly smaller.

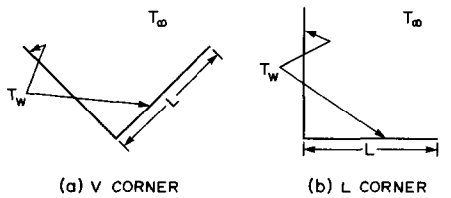

FIG. 1. The investigated corner configurations.

Although Fig. 1 suggests that the investigated physical situation is two-dimensional (i.e. the dimension normal to the plane of the figure is not shown), the absence of three-dimensional effects cannot be taken for granted. The width W of the corner in the direction normal to the plane of the figure is necessarily finite. If the corner were open to the fluid environment at the extremities of its width, fluid might pass through the open ends, giving rise to potential end effects. The possible influence of end effects was investigated in two ways. First, for corner configurations open at the extremities of the width, Nusselt number data corresponding to a fixed Rayleigh number were collected for different aspect ratios L/W (length/width). Second, for each geometrical configuration investigated (i.e. each type of corner and each plate length L), a complete set of experimental data was collected for the case in which the extremities of the width were blocked. These data supplemented those collected with the extremities open.

All told, then, twelve different versions of the experimental apparatus were employed: two types of corners, three lengths L per corner type, and open or blocked extremities per corner and per length.

For each configuration, the wall-to-ambient temperature difference was varied parametrically over a range which generally encompassed 1–10°F. For the V corner, where symmetry prevails for the two plates which form the corner, the average Nusselt number applicable to either plate was determined. For the L corner, separate determinations were made for the Nusselt numbers of the horizontal and vertical plates, as well as for the average for the two plates. Tight algebraic correlations of the Nusselt number results were obtained for all cases. In the presentation of results, particular attention will be given to the possible role of end effects, and comparisons will be made

NOMENCLATURE

A	plate surface area	T_w	temperature of heated walls
c_p	specific heat	T_∞	ambient temperature
g	acceleration of gravity	W	width of corner (normal to plane of Fig. 1).
h	heat transfer coefficient, $Q/A(T_w-T_\infty)$		
k	thermal conductivity		
L	length of each heated wall forming the corner (Fig. 1)	Greek symbols	
Nu_L	Nusselt number, hL/k	β	coefficient of thermal expansion
Q	rate of heat transfer	μ	viscosity
Ra_L	Rayleigh number, $[g\beta(T_w-T_\infty)L^3/\nu^2](c_p\mu/k)$	ν	kinematic viscosity
		ρ	density.

of the Nusselt numbers for the cases in which the extremities of the corner were either open or blocked.

The presentation of results will also include the timewise variation of the Nusselt number. Both T_w and T_∞ tended to vary with time throughout the duration of a data run, but the temperature difference (T_w-T_∞) was independent of time after a brief transient period subsequent to the onset of heating. Since the heat input was constant at all times, the Nusselt number was also constant following the brief initial transient.

The heat transfer experiments were supplemented by flow visualization studies. The flow visualization was performed by means of an electrochemical technique which gave rise to local changes in the pH of the water bath in which the apparatus was situated. The pH changes triggered a change in color of a pH indicator, thymol blue, which had been added to the water along with minute amounts of other pH-regulating chemicals. The fluid colored by the pH change served as a tracer to reveal the pattern of fluid flow.

With regard to the literature, it appears that the focus of the prior work on natural convection in corners has been the corner formed by the intersection of two vertical walls at right angles. For that case, experimentally determined heat transfer results are presented in ref. [1], while analytical and numerical results were obtained in ref. [2] and in refs. [3, 4], respectively.

EXPERIMENTAL APPARATUS AND PROCEDURE

Overview

The experiments were performed for corner configurations having heated walls of length L (Fig. 1) equal to 5.08, 10.16, and 15.24 cm (2, 4, and 6 in.). For all cases, the spanwise width W of the heated walls (normal to the plane of Fig. 1) was 30.48 cm (12 in.). The sequence of the experiments was initiated with the $L = 15.24$ cm (6 in.) walls for which four distinct sets of heat transfer experiments were carried out. The first of these was the V corner with open spanwise extremities, followed by the V corner with blocked spanwise extremities. Then, after appropriate alterations, heat transfer experiments for the L corner were performed, successively with open and closed spanwise extremities.

Next, the plates which served as the heated walls were machined in a vertical milling machine to reduce their lengths from $L = 15.24$ to 10.16 cm (6 to 4 in.). The apparatus was then reassembled, and four sets of heat transfer experiments, similar to those described in the foregoing paragraph, were carried out. Once those experiments had been completed, the plates were milled once again to reduce their lengths from $L = 10.16$ to 5.08 cm (4 to 2 in.), after which the same four sets of heat transfer experiments were performed.

The flow visualization study was initiated after all of the heat transfer data runs had been completed. This ordering of the experiments was chosen because of concern that the chemicals added to the water bath to facilitate the visualization work would etch the surfaces of the heated plates and/or corrode the heating circuitry. As a consequence of this ordering, the flow visualization was performed only for the corner with $L = 5.08$ cm (2 in.) heated walls.

From the foregoing discussion, it is evident that the $L = 15.24$ cm (6 in.) corner is the primary corner configuration, and that the $L = 5.08$ and 10.16 cm (2 and 4 in.) corners are derivatives. Therefore, in the description of the apparatus which follows, primary attention will be given to the $L = 15.24$ cm (6 in.) corner.

Apparatus details

A cross-sectional view of the $L = 15.24$ cm (6 in.) corner assembly is presented in Fig. 2. The assembly is shown in the V corner configuration, but, after a 45° rotation, the same diagram applies for the L corner configuration. The support systems for the two configurations are different and will be described later.

As seen in Fig. 2, the corner assembly consisted of the heated plates which formed the corner, a trough-like brace which cradled the heated plates, a block of insulation the upper face of which was recessed to receive the plates and the brace, and a tray which

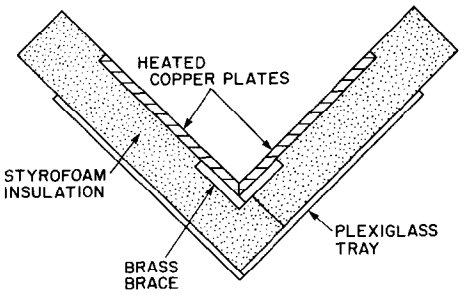

FIG. 2. Cross-sectional view of the V corner assembly (L = 15.24 cm (6 in.)).

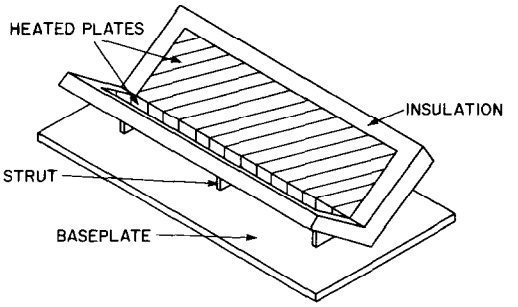

FIG. 3. Experimental setup for the open-ended V corner.

facilitated the interfacing of the assembly with the support system. The heated plates were of copper, chosen for its high thermal conductivity. Each of the two copper plates was 0.635 cm ($\frac{1}{4}$ in.) thick. The exposed surface of each plate was a 15.24 × 30.48 cm (6 × 12 in.) rectangle ($L \times W$) which was polished to a smooth finish with 900-grit aluminum oxide lapping compound. The contacting edges of the plates were beveled at 45° to facilitate formation of the 90° corner.

Twenty-one shallow grooves were machined into the rear surface of each plate to accommodate electrical-resistance heating wire (0.010 in. Teflon-coated chromel wire). For each plate, the heating wire was arranged in three altogether independent circuits. One circuit occupied the first third of the 15.24 cm (6 in.) plate length, another circuit occupied the second third, and the last circuit occupied the final third. Because of this arrangement, each reduction of the plate length by machining resulted in the removal of an entire circuit but left the remaining circuits intact.

The temperature of each plate was measured with the aid of ten fine-gauge, precalibrated thermocouples. The thermocouples were made from 0.010-in.-diameter Teflon-coated chromel and constantan wire, chosen because of inertness in water and high thermoelectric sensitivity. The thermocouples penetrated the plate from the rear, and the junctions were positioned about 0.05 cm (0.02 in.) from the exposed face.

The trough-like brace served as a rigid foundation for the heated copper plates and also provided a means of ensuring that the plates intersected at right angles. The brace was made from a pair of 0.635 cm ($\frac{1}{4}$ in.) thick brass plates, all of whose surfaces were painstakingly machined to achieve parallelism and squareness. Screws were used to hold the plates together. Grooves were milled into the upper faces of the brace to accommodate the wires which emanated from the rear faces of the heated plates.

Extraneous heat losses from the corner were virtually eliminated by seating it in a block of water-tolerant, closed-pore polystyrene (Styrofoam), as illustrated in Fig. 2. The insulation system was formed by bonding together two 5.08-cm-thick (2 in.) sheets of Styrofoam at right angles, with silicon rubber serving as the bonding agent. Recesses were machined into the upfacing surfaces of the insulation to accommodate the heated plates and the support brace. As seen in Fig. 2, the insulation extended 5.08 cm (2 in.) beyond all the outboard edges of the heated plates, thereby minimizing extraneous heat losses at the edges. The exposed surfaces of the heated plate and the framing insulation were coplanar.

A V-shaped tray made of 0.312-cm-thick ($\frac{1}{8}$ in.) plexiglass plates was used to facilitate the interfacing of the corner assembly with the support system. The tray was bonded to the rear face of the insulation by silicon rubber.

The support system consisted of three V-shaped plexiglass struts rigidly attached to a plexiglass baseplate. The struts were bonded to the tray by silicon rubber. A leveling leg was provided at each corner of the baseplate to facilitate the proper alignment of the corner. Brass weights were placed on the baseplate to prevent the assembly from floating due to the low density of the polystyrene insulation.

Figure 3 shows the fully assembled V corner and its support. Note that in the configuration shown in Fig. 3, the spanwise extremities of the corner are open (i.e. unblocked).

As indicated earlier, one of the issues of concern here is the possible influence of end effects on the heat transfer results. To examine this issue, supplementary experiments were performed in which the streamwise extremities were blocked by triangular-shaped inserts made of Styrofoam. The experimental setup with these barriers in place is shown schematically in Fig. 4. The barriers were 5.08 cm (2 in.) thick and rested on the surface of the insulation which extended beyond the ends of the heated plates. Silicon rubber

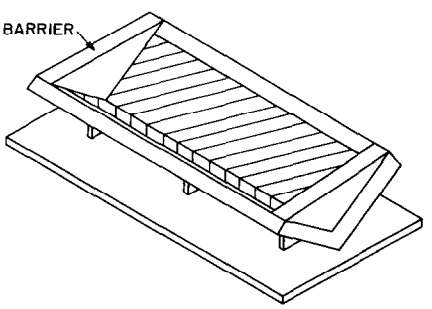

FIG. 4. End closure for the V corner.

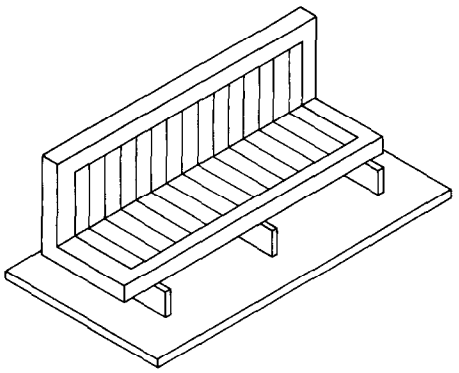

FIG. 5. Experimental setup for the open-ended L corner.

was used to seal the barriers to the surface of the insulation.

The foregoing discussion has been focused on the $L = 15.24$ cm (6 in.) V corner. The corresponding L corner differed only in the nature of the support structure and in certain aspects of the plate heating and ambient thermocouple arrangements. A schematic diagram of the experimental setup for the L corner with open (i.e. unblocked) extremities is presented in Fig. 5. The corner was supported by plexiglass bars on which the horizontal wall of the corner rested. The bars were 10.16 cm (4 in.) high. For the investigation of possible end effects for the L corner, the utilized barriers were those already described for the V corner.

The $L = 10.16$ and 5.08 cm (4 and 2 in.) corners were obtained by successive reductions in the length dimension of the heated plates, while maintaining the width W at 30.48 cm (12 in.). For all three investigated lengths, the 5.08 cm (2 in.) insulation extension which framed the heated surfaces was maintained.

The heating circuits were powered by d.c. current. For the V corner, several individual heating circuits (for both heated plates) were connected in parallel across a single d.c. power supply. This heating arrangement was sufficient to yield nearly uniform wall temperature, with deviations of individual wall temperature readings from the mean being typically about 2% of the wall-to-ambient temperature difference.

In the case of the L corner, the attainment of temperature uniformity within the aforementioned tolerance required the use of three power supplies. One power supply fed the parallel-wired heating circuits of the horizontal plate. A second supply powered the uppermost heating circuit of the vertical plate, while the third supply fed the other circuits of the vertical plate.

Fluid environment

The experiments were performed with the heated corner situated in a thermally guarded water bath, with the baseplate positioned on the floor of the tank in which the water was contained. The thermal guarding was achieved by a tank-in-tank arrangement. Both tanks were fabricated from plexiglass, with respective dimensions of $61 \times 61 \times 51$ cm and $81 \times 81 \times 56$ cm ($24 \times 24 \times 20$ in. and $32 \times 32 \times 22$ in.), length $\times$ width $\times$ depth. The inner tank, which served as the thermal environment for the heat transfer experiments, was filled with distilled water. Distilled water was also used to fill the space between the tanks, in which was situated a temperature control and water circulation unit. Heat and moisture losses from the inner-tank and intertank water surfaces were suppressed by Styrofoam insulation equipped with a moisture barrier.

Prior to the initiation of a given experiment, both temperature uniformity throughout the inner-tank water bath and temperature equality of the inner-tank and intertank water were achieved. This guaranteed the absence of extraneous motions in the fluid ambient of the corner prior to the beginning of the experiment.

A vertical array of three thermocouples was used to measure the temperature in the water bath in which the corner was situated. The lowermost of the thermocouples was placed at the lowest position from which the corner could draw fluid. Thus, for the open-ended V corner, the lowest thermocouple was positioned at the same level as the intersection of the two heated plates (i.e. the apex of the V). On the other hand, for the closed-ended V corner, the lowest thermocouple was at the same level as the top of the barrier which closed the ends. In the case of the L corner, the lowest thermocouple was positioned at the same elevation as the surface of the horizontal member of the corner.

The middle and upper thermocouples were, respectively, positioned 7.6 and 15.2 cm (3 and 6 in.) above the lowest thermocouple. The thermocouple array was situated 10–15 cm (4–6 in.) to the side of the outboard extremity of the corner assembly. This placement avoided direct impingement of the buoyant upflow from the corner on the thermocouples.

All thermocouple voltages were read to 1 μV with a programmable, scanning datalogger. The rapid sensing capability of the datalogger proved to be advantageous because the wall and ambient temperatures tended to increase with time, although the wall-to-ambient temperature difference became constant after an initial transient period.

Flow visualization

As noted earlier, the flow visualization experiments were performed after all of the heat transfer data had been collected. The flow pattern was made visible by an electrochemical technique. To prepare the water bath for the visualization experiments, a pH indicator, thymol blue powder, was dissolved and then added to the water. Then, sodium hydroxide was introduced in amounts sufficient to attain the end point, as indicated by the deep blue color of the water solution. Hydrochloric acid was then added to increase the acidity and change the color of the solution to reddish-yellow.

The basic idea of the visualization technique is to apply a small d.c. voltage (4–6 V) across two elec-

trodes situated in the just-described electrochemical solution. At the negative electrode, the change of pH due to the current flow brings about a local color change from reddish-yellow to blue. The blue fluid, being neutrally buoyant, faithfully follows the natural convection motions.

For the investigation of the fluid flow patterns for the V and L corners, the heated plates themselves served as the negative electrodes (i.e. the sites where the blue fluid was generated). To obtain supplementary information for the V corner, a wire probe was also used as the negative electrode. The positive electrode was a copper plate situated on the floor of the containment tank. A d.c. power supply was used to drive the electrochemical current flow. A voltage below 4 V did not generate sufficient marked fluid to clearly delineate the flow pattern, while voltages greater than 6 V produced unwanted hydrogen bubbles at the negative electrode. These characteristics limited the applied voltage to the 4–6 V range.

RESULTS AND DISCUSSION

Data reduction

The Nusselt numbers were evaluated from the defining equations

$$h = Q/A(T_w - T_\infty), \quad Nu_L = hL/k. \tag{1}$$

For the V corner, thermal symmetry prevailed as witnessed by the fact that for the same heat input to each of the plates, the resulting temperatures of the two plates were the same. Thus, for the V corner, Q in equation (1) was evaluated as the sum of the heat inputs to the plates and A was the sum of the surface areas. In addition, T_w was the mean surface temperature (averaged over the thermocouples of both plates) and T_∞ was the mean ambient temperature (average of the three thermocouples in the water bath). The thus-evaluated Nu pertain equally well to the individual plates and to the two-plate average.

For the L corner, separate values of the Nusselt number were determined for the horizontal and vertical plates and for the average of the two plates. For the individual plates, Q, A, and T_w were the heat input, surface area, and mean surface temperature for each plate. For the two-plate average Nusselt number, Q was the sum of the heat inputs, A the sum of the surface areas, and T_w the average of the thermocouple readings for the two plates. The surface temperatures for the two plates were virtually identical. As before, T_∞ was the average of the three waterbath thermocouples.

The Nusselt number results will be displayed as a function of the Rayleigh number

$$Ra_L = [g\beta(T_w - T_\infty)L^3/\nu^2](c_p\mu/k) \tag{2}$$

where T_w and T_∞ were determined as described in the foregoing.

The thermophysical properties k, ρ, β, μ, and c_p appearing in Nu and Ra were evaluated at a reference temperature $(T_w + T_\infty)/2$. Algebraic descriptions of k, ρ, μ, and c_p for water are presented in Section 4.1.2 of ref. [5], and β was determined by differentiation of the equation for ρ. The literature sources from which the properties were taken are: k [6], ρ [7], μ [8], and c_p [9].

It was noted in the Introduction that a true steady state was not achieved and that the heat transfer results were quasi-steady. To illustrate this state of affairs, Fig. 6 has been prepared. This figure corresponds to the open-ended V corner, but the trends in evidence in the figure pertain to all of the investigated cases. In the figure, Nu_L is plotted as a function of time for parametric values of Ra_L, where time = 0 denotes the onset of heating. The black and open data symbols respectively correspond to the $L = 5.08$ and 15.24 cm (2 and 6 in.) corners.

From an examination of the figure, it is seen that after a brief initial period of decrease, Nu_L becomes altogether independent of time. In virtually all cases, the invariance of Nu_L is in evidence for times of 15 min and greater and, in some cases, the invariance sets in earlier.

During a given experiment, the heat input was altogether constant, while both T_w and T_∞ varied with time. The attainment of time-invariant Nusselt numbers occurred because the variations of T_w and T_∞ were identical, so that $(T_w - T_\infty)$ was perfectly constant.

The Nusselt numbers to be reported here are those from the time-invariant period. Strictly speaking, these are quasi-steady Nusselt numbers. However, considering the slowness of the variations of T_w and T_∞, it is reasonable to regard these Nusselt numbers as identical to steady-state values.

Results for the V *corner*

The first set of Nusselt number results to be presented are for the open-ended V corner, and Fig. 7(a) has been prepared for this purpose. The figure contains data for all three plate lengths, which yield an overall range of Ra_L from 2×10^6 to 1.6×10^9. The data from the various plate lengths overlap, and in the regions of overlap there is generally good agreement. Since the L/W ratios for the three plate lengths are different (because W is a constant) and since the end effects, if any, should respond to L/W, it would appear that end effects were minimal in the investigated range.

The data were not very well fitted by a single correlating line. A least-squares fit

$$Nu_L = 0.229 Ra_L^{0.306} \tag{3}$$

was examined. Of the data, 78% fell within $\pm 5\%$ of the line, and the maximum deviation was 8.1%.

There appears to be a change of slope of the data at $Ra_L = 5.6 \times 10^7$, suggesting a flow transition. For the range between 2×10^6 and 5.6×10^7, a least-squares fit yielded

$$Nu_L = 0.398 Ra_L^{0.271} \tag{4a}$$

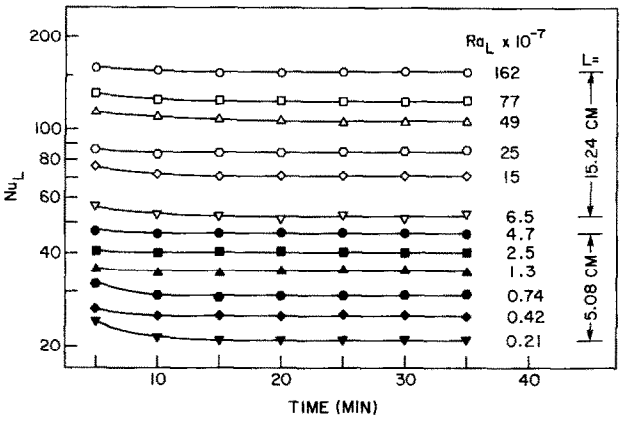

FIG. 6. Time history of the Nusselt number (open-ended V corner).

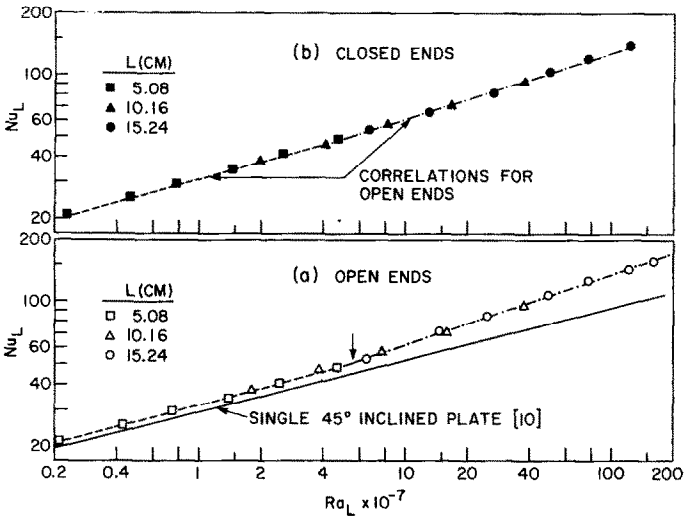

FIG. 7. (a) Nusselt numbers for the open-ended V corner and comparisons with the 45°, single inclined plate. (b) Nusselt numbers for the closed-ended V corner and comparisons with those for the open-ended V corner.

while a preassigned $\frac{1}{4}$-power fit led to

$$Nu_L = 0.570 Ra_L^{1/4}. \quad (4b)$$

For both fits, 57% of the data fell within $\pm 2\%$ of the correlation, with respective maximum deviations of 3.4 and 4%.

For the Ra_L range between 5.6×10^7 and 1.6×10^9, the counterparts of equations (4) are

$$Nu_L = 0.116 Ra_L^{0.340} \quad (5a)$$

and

$$Nu_L = 0.132 Ra_L^{1/3}. \quad (5b)$$

Equation (5a) correlates 55% of the data within $\pm 2\%$, with the maximum deviation being 3.6%. For equation (5b), the $\pm 2\%$ band encompasses 45% of the data, and the maximum deviation is 3.3%.

The dashed lines appearing in Fig. 7(a) represent equations (4a) and (5a), and the arrow indicates the break point between the two equations. Although there is no particular reason to prefer the force fits (1/4 and 1/3 exponents) over the naturally occurring exponents (0.271 and 0.340), they (i.e. the former) are suggestive of certain flow regimes and of a transition between these regimes.

Further information about the possible role of end effects is conveyed in Fig. 7(b). In that figure, the data points correspond to the situation in which barriers blocked the spanwise extremities of the V corner, as illustrated in Fig. 4. The dashed lines, on the other hand, depict equations (4a) and (5a), which are the correlating equations for the open-ended corner. From the figure, it is seen that truly excellent agreement prevails between the closed-end data and the open-end correlation. This agreement provides strong evidence for the absence of end effects.

It is relevant to compare the present Nusselt numbers for the V corner with those for a single, upfacing plate inclined at 45° to the horizontal. The latter results are available in ref. [10] and are plotted as a solid line in Fig. 7(a). As seen in the figure, the Nu_L values for the V corner exceed those for the single

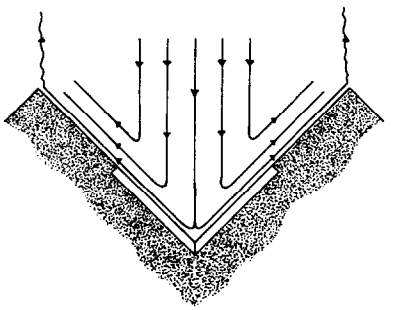

FIG. 8. Flow visualization for the V corner.

plate over the entire investigated range of Ra_L. At the low end of the range, the corner Nu_L values exceed the single-plate Nu_L values by about 5%, while at the high end of the range the corner values are about 50% high.

It is believed that the key factor in the aforementioned comparison is the persistence of laminar flow on the single plate for the entire Ra_L range. This is evidenced by the $\frac{1}{4}$-power slope of the single-plate line. On the other hand, the V corner data indicate a transition to turbulence at about $Ra_L = 5.6 \times 10^7$. Beyond that Ra_L, the two sets of data exhibit ever-increasing deviations.

Flow visualization for the V corner was performed with the aid of the electrochemical technique which was described earlier. The visualization experiments were carried out after all of the heat transfer data had been collected and, because of this, visualization results were obtained only for the $L = 5.08$ cm (2 in.) corner.

A schematic diagram of the pattern of fluid flow in the V corner is presented in Fig. 8. This figure is based on extensive visual observations. The visualization revealed a symmetric, two-dimensional flow pattern. Downflowing fluid enters the corner from above. Upon reaching the immediate neighborhood of the heated plates, the downflow turns and moves outward along the plates. In general, as witnessed by the spacing of the streamlines, the velocities adjacent to the walls are much higher than those in the core of the flow.

As the outflowing fluid passes over the insulation that extends beyond the heated plates, it continues to flow more or less parallel to the surface. Upon reaching the trailing edge of the insulation, the flow separates from the surface and rises vertically in a wavy pattern.

Results for the L *corner*

The Nusselt number results for the L corner are presented in Fig. 9(a). The figure contains separate sets of data for the horizontal and vertical walls of the corner and for the average of the two walls (circle, square, and triangle data symbols, respectively). Each set of data includes the three investigated wall lengths —5.08, 10.16, and 15.24 cm (2, 4, and 6 in.). The lines passing through the data are least-squares fits, as will be discussed shortly.

As seen in the figure, the Nusselt numbers for the horizontal wall of the L corner exceed those for the vertical wall of the corner over the entire investigated range of Ra_L. The deviations between the horizontal-wall and vertical-wall Nusselt numbers increase as Ra_L increases—from 8 to 50% as Ra_L increases from 3×10^6 to 5×10^8. From circumstantial evidence gleaned from the exponent of the *Nu–Ra* relation, it appears that the horizontal wall is washed by a turbulent flow, while the vertical wall is washed by a laminar flow. This conjecture, if true, would account for the growing deviations between the two sets of Nusselt numbers.

Two other possible factors may be cited to account for the higher *Nu* values for the horizontal wall. One is that the vertical wall is washed by fluid which may have been preheated by having previously passed over the horizontal wall. This preheating may reduce the vertical-wall Nusselt numbers. The second is that the flow induced by the buoyancy at the vertical wall passes, at least in part, over the horizontal wall, tending to increase the Nusselt numbers there.

Attention will now be turned to the algebraic description of the data. Each set of data was fit with two equations, one a least-squares representation and the other a fit with an assigned exponent. For the horizontal wall, the two equations are, respectively

$$Nu_L = 0.131 Ra_L^{0.349}, \quad Nu_L = 0.172 Ra_L^{1/3}. \quad (6)$$

The first of these correlates 71% of the data within $\pm 2\%$, with the maximum deviation being 2.9%. For the second correlation, 59% of the data are within $\pm 2\%$, and the maximum deviation is 5.4%.

For the vertical wall, the correlating equations are

$$Nu_L = 0.347 Ra_L^{0.280}, \quad Nu_L = 0.588 Ra_L^{1/4}. \quad (7)$$

Within a $\pm 2\%$ band, the first equation correlates 65% of the data; the maximum deviation is 4.2%. The $\frac{1}{4}$-power fit gives a considerably less accurate correlation: 59% of the data within $\pm 5\%$ and a maximum deviation of 9.4%.

The correlations for the two-plate average are

$$Nu_L = 0.201 Ra_L^{0.318}, \quad Nu_L = 0.154 Ra_L^{1/3}. \quad (8)$$

All of the data lie within $\pm 1.9\%$ of the first equation, while 53% of the data lie within $\pm 2\%$ of the second equation. The maximum deviation of the data from the latter equation is 4.3%.

Further inspection of Fig. 9(a) shows that in Ra_L ranges where the data from plates of different length overlap, there is good but not perfect agreement. Thus, on this basis, it appears that the results may have been slightly influenced by end effects. This issue will be revisited shortly.

The Nu_L data for the vertical wall of the L corner are compared with the Nusselt numbers for a single isothermal vertical plate in Fig. 9(b). The latter are taken from the correlation of ref. [11]. At the low end of the *Ra* range, the L-corner Nusselt numbers are about 15% below those for the single plate, while at

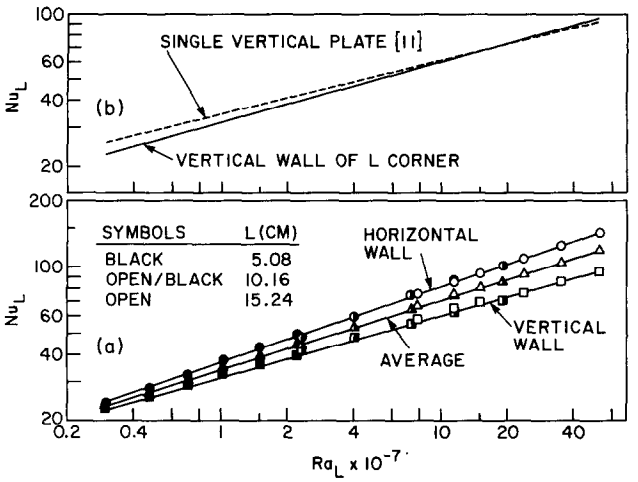

FIG. 9. (a) Nusselt numbers for the open-ended L corner. (b) Comparison of Nusselt numbers for the vertical wall of the L corner with those for a single vertical plate.

the high end of the range, the former are a few percent above those for the latter. It is believed that the low-end ordering is influenced by the aforementioned preheating sustained by the fluid prior to encountering the vertical wall of the corner. At the high end, the preheating effect is probably moderated by the heightened entrainment of fresh fluid from the ambient into the boundary layer of the vertical wall.

Comparisons of the Nu values for the horizontal wall of the corner with those for a single horizontal plate will now be considered. The latter results are from a correlation given in ref. [12], in which the characteristic length is the ratio of the surface area to the perimeter of the plate. When the Nusselt number correlation of ref. [12] is converted to Nu_L and Ra_L, the length/width ratio L/W of the plate emerges. Since the three corners employed here had different L/W ratios, each of the three corners will be compared separately with the single plate results.

The correlation of ref. [12] for the single horizontal plate may be interpreted in two ways for the purposes of the comparison. First, the correlation may be evaluated for a horizontal plate of dimensions $L \times W$. In addition, a plate of dimensions $2L \times W$ can also be considered since its centered plume appears to be similar to the upwelling fluid adjacent to the vertical plate of the L corner.

The comparisons are presented in Figs. 10(a)–(c), which respectively pertain to the 5.08, 10.16, and 15.24 cm (2, 4, and 6 in.) corners. In each figure, different types of lines are used to represent the present corner results and those of ref. [12] for the single plate. Note that the breaks in the latter lines are due to specification in ref. [12] of different correlating equations for laminar and turbulent flow. When the lines for the $L \times W$ and $2L \times W$ plates overlap, the merged lines are represented by a composite of the two.

If the $2L \times W$ single plate is taken as the standard of comparison, Figs. 10 indicate that the Nusselt numbers for the horizontal wall of an L corner are greater

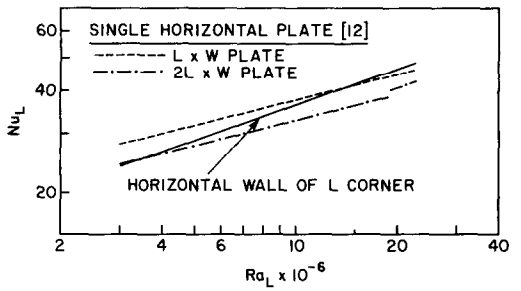

FIG. 10(a). Comparison of Nusselt numbers for the horizontal wall of the L corner with those for a single horizontal plate; L = 5.08 cm (2 in.).

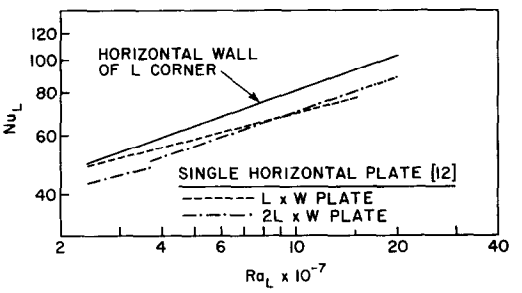

FIG. 10(b). Comparison of Nusselt numbers for the horizontal wall of the L corner with those for a single horizontal plate; L = 10.16 cm (4 in.).

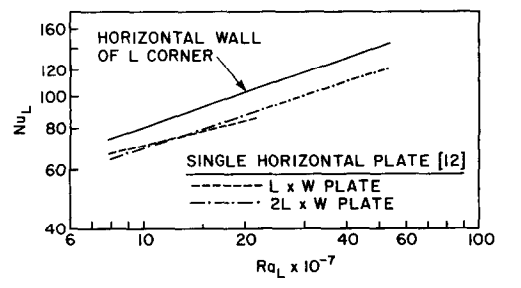

FIG. 10(c). Comparison of Nusselt numbers for the horizontal wall of the L corner with those for a single horizontal plate; L = 15.24 cm (6 in.).

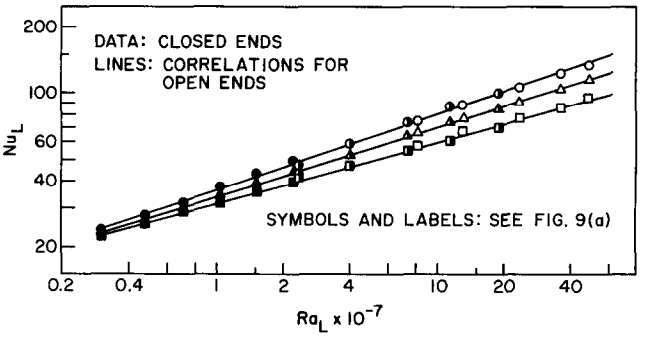

FIG. 11. Nusselt numbers for the closed-ended L corner and comparisons with those for the open-ended L corner.

than those for a single horizontal plate. The same conclusion applies for the comparison based on the $L \times W$ single plate, for the two longer plates. The higher Nu values at the horizontal wall of the corner are believed to be due to the buoyancy created at the vertical wall of the corner. The flow induced by the buoyancy at the vertical wall, in part, passes over the horizontal wall en route to the vertical wall. This flow, which is additional to that induced at the horizontal wall of the corner, should enhance the heat transfer there.

The issue of possible end effects, already discussed in connection with Fig. 9(a), will now be reconsidered. Figure 11 presents Nu_L data for the L corner with blocked ends, with the blockage being accomplished by the use of barriers such as those depicted in Fig. 4. Also appearing in the figure are the correlating lines for the case of the open-ended L corner.

Inspection of Fig. 11 indicates that the closed-end Nu_L data are well correlated by the lines which represent the open-end case. Indeed, the relationship between the data and correlating lines is more or less the same in Figs. 9(a) and 11. Since the closing of the ends by barriers should alter the end effects, if they are significant, it may be concluded that the Nu_L data were not materially influenced by end effects.

Attention will now be turned to the flow visualization for the L corner. The visualization experiments were performed for the open-ended case and for the smallest plate length ($L = 5.08$ cm (2 in.)). The heated copper plates served as the electrodes at which the blue tracer fluid was generated. Figure 12 is a sketch of the observed flow pattern.

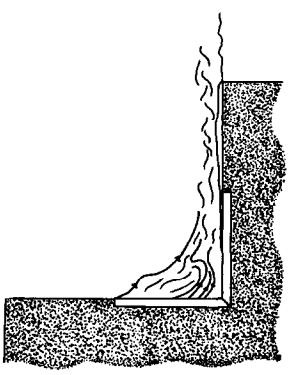

FIG. 12. Flow visualization for the L corner.

As expected, the fluid which passes over the horizontal wall of the corner is drawn toward the vertical wall. In particular, the plume rising from the horizontal wall is highly skewed in the direction of the vertical wall. As the plume rises, it experiences instabilities which are manifested as waviness in the 'dye' stream. A thin boundary layer forms at the surface of the vertical wall. The thickness of the boundary layer increases with height along the heated plate. The boundary layer remains attached to (i.e. unseparated from) the surface of the insulation which extends vertically upward from the heated plate.

The visualized flow pattern supports the explanations set forth earlier in connection with comparisons of the vertical- and horizontal-wall Nu_L values and with comparisons of these Nu_L with their single-plate counterparts.

CONCLUDING REMARKS

Natural convection in V- and L-shaped corners has been investigated here by experiment using water as the heat transfer medium. Quantitative information, expressed in algebraic form, is presented for the variation of the Nusselt number with the Rayleigh number. It was found that the Nusselt numbers at the walls of the V corner exceeded those for a single inclined plate. Similarly, the Nusselt numbers at the horizontal wall of the L corner were greater than those at a single horizontal plate. On the other hand, for the vertical wall of the L corner, an opposite relation existed over an appreciable portion of the investigated Rayleigh number range.

It remains to compare the two types of corners. At Rayleigh numbers of 5×10^6, 5×10^7, and 5×10^8, the corresponding average Nusselt numbers for the V and L corners are (26.0, 27.1), (48.6, 56.4), and (105.2, 117.3). Thus, the L corner provides higher values of the Nusselt number than does the V corner. This outcome may be explained by the expected easier access of the ambient fluid to the inter-corner space for the case of the L configuration.

REFERENCES

1. J. H. Van Leeuwen, C. M. Looman and J. Schenk, Experimental study of velocity and temperature distribution for free convection in a corner, *Int. J. Heat Mass Transfer* **14**, 561–564 (1971).
2. D. S. Riley and G. Poots, Thermal convection in a heated vertical corner, *Q. J. Mech. Appl. Math.* **25**, 401–421 (1972).
3. K. Ramakrishna, Natural convection along corners and rectangular ducts, Ph.D. Thesis, Department of Mechanical and Aerospace Engineering, Polytechnic Institute of New York (1980).
4. S. G. Rubin and B. Grossman, Viscous flow along a corner, numerical solution of the corner layer equations, *Q. J. Appl. Math.* **29**, 169–186 (1971).
5. R. Ruiz, Natural convection heat transfer in partially enclosed configurations, Ph.D. Thesis, Department of Mechanical Engineering, University of Minnesota (1986).
6. Y. S. Touloukian, P. E. Liley and S. C. Saxena, *Thermophysical Properties of Matter—Conductivity*, Vol. 3. IFI/Plenum, New York (1970), updated (1981).
7. G. S. Kell, Effects of isotropic composition, temperature, pressure, and dissolved gases on the density of liquid water, *J. Phys. Chem. Reference Data* **6**, 1115 (1977).
8. A. Nagashima, Viscosity of water substance—new international formulation and its background, *J. Phys. Chem. Reference Data* **6**, 1159–1160 (1977).
9. Y. S. Touloukian and T. Makita, *Thermophysical Properties of Matter—Specific Heat*, Vol. 6. IFI/Plenum, New York (1970), updated (1981).
10. T. Fujii and H. Imura, Natural convection heat transfer from a plate with arbitrary inclination, *Int. J. Heat Mass Transfer* **15**, 755–767 (1972).
11. S. W. Churchill and H. H. S. Chu, Correlation equations for laminar and turbulent free convection from a vertical plate, *Int. J. Heat Mass Transfer* **18**, 1323–1329 (1975).
12. J. R. Lloyd and W. R. Moran, Natural convection adjacent to horizontal surface of various planforms, *J. Heat Transfer* **96**, 443–447 (1974).

CONVECTION NATURELLE DANS DES ANGLES EN FORME DE V ET DE L

Résumé—Des expériences ont été faites pour étudier la convection naturelle dans deux types d'angle. L'un, l'angle en V, est formé de deux plaques inclinées à 45°, faisant face vers le haut, chauffées et se coupant à 90°. L'autre, le coin en L, est formé par une plaque horizontale chaude, tournée vers le haut qui intersecte une plaque chaude verticale. Dans les deux cas, les deux plaques ont la même température uniforme qui peut varier paramétriquement. Les variations de la différence de température entre la surface et l'ambiance, et de la longueur de plaque, conduisent à un domaine de nombre de Rayleigh entre $2 \cdot 10^6$ et $1{,}5 \cdot 10^9$. Des modifications de l'appareil sont faites pour étudier le rôle possible des effets d'extrémité. Les expériences thermiques sont complétées par des visualisations d'écoulement. Les nombres de Nusselt pour tous les cas sont traduits en formules de loi-puissance du nombre de Rayleigh. Les valeurs du nombre de Nusselt aux parois de l'angle en V et à la paroi horizontale de l'angle L sont supérieures à celles relatives aux plaques uniques.

NATÜRLICHE KONVEKTION IN V- UND L-FÖRMIGEN ECKEN

Zusammenfassung—In Experimenten wurde die natürliche Konvektion in zwei verschiedenen Eckanordnungen untersucht. Die V-förmige Ecke wird durch zwei beheizte, nach oben zeigende Platten gebildet, die jeweils um 45 Grad zur Horizontalen geneigt sind und zwischen sich einen Winkel von 90 Grad einschließen. Die L-förmige Ecke besteht aus einer horizontalen und einer vertikalen Platte. In beiden Fällen sind die Plattenoberflächen isotherm; die Temperatur wird als Parameter verändert. Durch Variation der Temperaturdifferenz zwischen Plattenoberfläche und Umgebung, sowie der Plattenlänge ergeben sich Rayleigh-Zahlen in einem Bereich von $2 \cdot 10^6$ bis $1{,}5 \cdot 10^9$. Der Versuchsaufbau wurde verändert, um auch mögliche Endeffekte zu untersuchen. Die Experimente zum Wärmeübergang wurden durch Sichtbarmachung der Strömung ergänzt. In allen Fällen kann die Nusselt-Zahl über einen Potenzansatz mit der Rayleigh-Zahl korreliert werden. Die Werte der Nusselt-Zahl an den Wänden der V-förmigen Ecken und an der horizontalen Wand der L-förmigen Ecke waren größer als jene der jeweiligen einzelnen Platte.

ЕСТЕСТВЕННАЯ КОНВЕКЦИЯ В V- И L-ОБРАЗНЫХ УГЛАХ

Аннотация—Проведено экспериментальное изучение естественной конвекции в углах двух типов: V и L. V-Образный угол образован двумя нагреваемыми взаимно перпендикулярными пластинами, обращенными рабочей стороной вверх и наклоненными к горизонтали под углом в 45°. L-Образный угол образован нагреваемой, обращенной рабочей стороной вверх горизонтальной пластиной, которая пересекается с нагреваемой вертикальной пластиной. Как в первом, так и во втором случае обе пластины имели одинаковую однородную температуру, которая изменялась параметрически. При изменениях разности температур поверхности и окружающей среды, а также длины пластин значения числа Рэлея изменялись в диапазоне от $2 \cdot 10^6$ до $1{,}5 \cdot 10^9$. Вносились также изменения в конструкцию установки для изучения возможного влияния концевых эффектов. Эксперименты по теплообмену проводились с одновременной визуализацией потока. Во всех случаях корреляции чисел Нуссельта и Рэлея описывались степенными зависимостями. Значения числа Нуссельта на стенках V-образного угла и на горизонтальной стенке L-образного угла превышали соответствующие значения для одиночных пластин.